JAAS

Accepted Manuscript

This is an *Accepted Manuscript*, which has been through the Royal Society of Chemistry peer review process and has been accepted for publication.

Accepted Manuscripts are published online shortly after acceptance, before technical editing, formatting and proof reading. Using this free service, authors can make their results available to the community, in citable form, before we publish the edited article. We will replace this *Accepted Manuscript* with the edited and formatted *Advance Article* as soon as it is available.

You can find more information about *Accepted Manuscripts* in the Information for Authors.

Please note that technical editing may introduce minor changes to the text and/or graphics, which may alter content. The journal's standard Terms & Conditions and the Ethical guidelines still apply. In no event shall the Royal Society of Chemistry be held responsible for any errors or omissions in this *Accepted Manuscript* or any consequences arising from the use of any information it contains.

ROYAL SOCIETY OF CHEMISTRY

www.rsc.org/jaas

JAAS

RSCPublishing

ARTICLE

Effect of N_2 on emission profile and excitation temperature in axially viewed plasma-ICP OES

Cite this: DOI: 10.1039/xoxxoooooox

Guilherme Luiz Scheffler and Dirce Pozebon*

Received ooth January 2012,
Accepted ooth January 2012

DOI: 10.1039/xoxxoooooox

www.rsc.org/

Fundamental studies were conducted in order to gain useful insights about energy transfer that takes place when a low flow (20 mL min^{-1}) of N_2 is introduced into the central channel of the Ar-ICP source in inductively coupled plasma optical emission spectrometry (ICP OES). Axial and radial emission profiles of Mg(I), Mg(II) and Ar(I) were collected along and across the central channel of both Ar-ICP and Ar-N_2-ICP. Axial profiles indicated a more energetic plasma close and above the load coil when N_2 was added. On the other hand, radial profiles suggested a wider and more uniform central channel with the N_2 flow addition. By computing the plasma robustness (Mg(II)/Mg(I) ratio) across the central ICP channel, it was found a low (and uniform) energy coupling among the bulk plasma and the central channel of the Ar-ICP, which was significantly improved by adding N_2. The results obtained also suggested that N_2 plays an important role locally, but does not in the outer regions of the ICP, which in turn denoted an unlikely N_2 diffusion. The better excitation conditions caused by N_2 were confirmed by measuring the excitation temperature in the central channel of the ICP, using a set of Fe ionic lines, where the excitation temperature increased from 7480K to 7910K. The effectiveness of the improved plasma robustness was evaluated for diluted seawater and the results demonstrated that the analyte signal suppression induced by the concomitants was reduced. Accuracy was accessed by analyzing certified reference samples (water and sediment), whereas good agreement among the concentrations found and those certified were observed. These results indicated low background and absence of spectral interferences caused by N_2. The estimated detection limits for both Ar-ICP and Ar-N_2-ICP were fairly comparable, revealing that the mixed-gas plasma is a robust source for trace elements determination using axially viewed-ICP OES. It was concluded that adding a low flow of N_2 is a simple way to increase plasma robustness without sacrificing analyte sensitivity.

Introduction

Inductively coupled plasma of Ar (Ar-ICP) has been successfully applied as an efficient dessolvation, vaporization, excitation and/or ionization source in ICP-spectrometry. This acceptance relies on the advantages of the Ar-ICP, such as high-temperature, inert environment, reduced chemical interferences, high energy for ionization, high excitation temperature and electron density. These good features justify the popular use of Ar in inductively coupled plasma optical emission spectrometry (ICP OES) and inductively coupled plasma mass spectrometry (ICP-MS) techniques. However, the widespread application of these techniques has shown limitations with respect to both spectroscopic and non-spectroscopic interferences.

Therefore, in an attempt to reduce such interferences and improve plasma characteristics in ICP-spectrometry, other gases with chemical and physical properties different of those of Ar have been investigated, particularly N_2. Mixed-gas plasmas like Ar-N_2-ICP have been utilized for fundamental studies or analytical application purposes since the launching of Ar-ICP in the late 1960s as reported by Montaser and others researchers.[1-6] Nitrogen has higher thermal conductivity and heat capacity than argon, which improve energy transfer in the plasma atmosphere. In fact, owing to the higher plasma robustness promoted by N_2, addition of this molecular gas has found valuable application to complex samples analysis such as undiluted seawater, soil digests, slurries and other matrices.[7-16] In addition, Ar-N_2-ICP proved usefulness in reducing oxides and Ar polyatomic ions, which are interferents in ICP-MS.[17-35]

Researches dealing with the use Ar-N_2-ICP in axially viewed plasma in ICP OES have been quite limited. Ohata *et al.*[36] demonstrated that plasma robustness (*i.e.,* Mg(II)/Mg(I) ratio) were improved by using 1.3% of N_2 in the outer gas,

whereas the robustness remained constant under higher amounts of N_2. These results corroborated with those found in the previous studies conducted by Montaser and Horlick. In a series of articles [1,37-40] these researchers reported that an excess of N_2 in the outer gas or nebulizer gas can degrade the plasma excitation capability and increase emission background. Scheffler and Pozebon[2] reported that the plasma robustness increased twice when 3.3% of N_2 was combined with the argon nebulizer flow. The authors demonstrated the usefulness of this approach for diminishing matrix effects induced by easily ionized elements such as Na, K and Ca, without impairing the limits of detection (LODs). However, ionic lines were mostly monitored and fundamental parameters of the ICP were not fully investigated. Investigations are necessary to understand how a low flow of N_2 acts in the analytical region of the plasma, *i.e.*, in its central channel. It is also important to investigate if there is any synergistic effect through the outer region or central channel of the ICP and how much N_2 is required for the robustness improvement without significant degradation of the LOD.

According to the aforementioned aspects, the purpose of the present study was the investigation of energy transfer that takes place when a small flow of N_2 is added into the central channel of an Ar-ICP. To this end, axially an vertically emission profiles of Mg(II), Mg(I), and Ar(I) were obtained. The characteristics of the Ar-N_2-ICP are demonstrated by the Mg(II)/Mg(I) intensity ratio, Ar emission signal and plasma excitation temperature, using Fe as thermometric species. Matrix effects caused by sea water (as a representative matrix) are investigated for a set of atomic and ionic energetic states. Possible shifts of the excitation/ionization processes induced by N_2 in the Ar-ICP are also investigated.

Experimental

Instrumentation, reagents, samples and solutions

The experiments were performed using an Optima 2000DV ICP OES spectrometer (Perkin Elmer, MA, USA), whereas the operating conditions are given in Table 1. Argon (99.996%, from White Martins/Praxair, Brazil) was used as plasma, auxiliary and nebulizer gas. Nitrogen (99.998%, from White Martins/Praxair, Brazil) was utilized to purge the optical system of the ICP OES spectrometer and as additional flow in the nebulizer gas. For liquid sample introduction into the ICP, a high-efficiency nebulizer with an aerosol desolvation unity was used (APEX-Q, from ESI, NB, USA). The system consists of a PFA nebulizer, a heated cyclonic spray chamber (140 ºC) and a Peltier multipass condenser (2 ºC), producing a partially dried aerosol and enhancing the sensitivity (about 30%). Nitrogen was added to the nebulizer gas through this system, as described elsewhere.[9] Calibration and test solutions were prepared by serial dilution of monoelemental stock solution (1000 mg L^{-1} - Merck, Darmstadt, Germany) or multielemental stock solution (10 mg L^{-1} SCP33MS - Quimilab, São José dos Campos, SP, Brazil). Deionised water (18.2 MΩ cm) purified in a Milli-Q system (Millipore, Billerica, MA, USA) was used for preparation of samples and solutions. Calibration solutions were prepared in 5% (v/v) HNO_3. Solutions containing 0.1 mg L^{-1} Mg or 50 mg L^{-1} Mg were used for plasma robustness evaluation and diagnostic emission line test, respectively. For plasma excitation temperature evaluation a 0.5 mg L^{-1} Fe solution was used. The reagents used - HCl (37% m/m), HF (48% m/m), HNO_3 (65% m/m) and H_2O_2 (30% m/m) - were purchased from Merck. The certified reference water NIST 1640a (trace elements in natural water, from National Institute of Standard and Technology - NIST, USA) was used to evaluate accuracy and possible spectral interferences caused by N_2. Other certified samples were also analysed for accuracy checking; pond sediment (NIES-2 from National Institute for Environmental Studies, Japan,), trace elements in river sediment (BCR-320 from Institute for Reference Materials and Measurements, Belgium,) and soil (NIST 2710a, Montana soil). These samples were decomposed as follows: 6 mL HNO_3 + 2 mL HF + 1 mL HCl + 1 mL H_2O_2 were added to 0.2 g of sample placed in PTFE vessel, which was subsequently closed and the mixture heated at 200 C for 6 h in a heating block. Then, the sample solution was transferred to a graduated polypropylene vial where the volume of the solution was elevated to 50 mL by adding water. Certified seawater (NASS-4 from National Research Council of Canada) was diluted as necessary and then spiked with the analytes (100 µg L^{-1}) for determining the extension of matrix effects. The instrument operating conditions used in the present study were similar to those established in a previous study[9] (rf power of 1500 W, nebulizer gas flow rate of 0.6 L min^{-1} and sample uptake rate of 0.65 mL min^{-1}). The N_2 flow rate was evaluated in the range of 0.0 to 20 mL min^{-1} and fixed at 20 mL min^{-1}, corresponding to 3.3% of the nebulizer gas. All experiments and samples were run in triplicate unless otherwise specified.

Emission profiles and excitation temperature

Axial spatial profiles were computed by measuring the emission intensity at different distances of the load coil (1 to 30 mm, with 1 mm of interval) whereas radial spatial profiles were computed across the plasma centre (from -15 mm to +15 mm, with 1 mm interval, being 0 mm the plasma center). The emission intensity signals were collected in both Ar-ICP and Ar-N_2-ICP) for comparison purposes. All data obtained were not treated using the Abel inversion in order to avoid additional uncertainties usually introduced by this mathematical procedure. In addition, the Abel inversion requires substantial modification of the commercial ICP OES instrument. The absolute emission intensity (I) of a set of ionic lines of Fe was used for calculating the plasma excitation temperature (T_{ex}) in the central channel axis of the ICP. The wavelength (λ), excitation energy (eV) and the transition probability (A) multiplied by the statistical weight of the respective emission level (*g*) are given in Table 2. It was assumed that both plasmas (Ar-ICP and Ar-N_2-ICP) were in local thermodynamic equilibrium (LTE) and the population of atoms and ions

followed the Boltzmann distribution (with k = $8.617x10^{-5}$ eV/K). In this way, by plotting ln(Iλ/gA) *versus* the corresponding excitation energy of the Fe lines, a linear relationship is obtained (slope = $-1/kT_{ex}$). Iron was selected as a thermometric species in view of its rich emission spectra, with a broad energy range, encompassing a short wavelength interval (avoiding correction for the detector response), appropriate intensity as well as signal-to-noise ratio. Additionally, transition probabilities for Fe are reliable and already well-known.

Results

Spatial profiles

Emission profiles collected across the ICP are useful to indicate possible changes of plasma characteristics and/or excitation pathways taking place in the ICP. In fact, collecting emitted photons is a passive process when compared to ion sampling using ICP-MS where the interface usually changes the ion population distribution in the ICP.[16] However, the emission profiles may be distorted by the skin effect (*i.e.*, the emission intensity in the central channel can be diluted/superposed by the hot plasma annulus), which is a disadvantage of ICP OES.[16] The emission intensity profiles of Mg(I), Mg(II) and Ar(I) collected across the ICP are shown in Fig. 1. By comparing Figs. 1(a) and (b), one can conclude that there are more excited ions than excited atoms in the central channel of the ICP under the N_2 flow. In such condition there is an overpopulation of Mg ionic states in the central channel of the ICP. As observed previously in laser ablation ICP-MS,[50] the normal analytical zone in the central channel of the ICP becomes broader and wider with the addition of N_2, in comparison to standard pure Ar-ICP. As observed in Fig. 1 (c) by the Ar emission profile, the molecular gas (N_2) reduces the excited Ar(I) population. One reason would be the increased population of more energetic Ar emission states, caused by the higher plasma temperature and/or charge transfer reaction among Ar and N^+ or N_2^+.[1,2,3]

Emission profiles collected along the ICP can indicate relevant aspects of particle vaporization, atomization or ionization along the plasma axis as well as possible matrix effects, earlier particle ionization and/or changes in the ICP characteristics. Fig. 2 shows the profiles obtained by plotting the emission intensity *versus* the observation height. From 0 to 5 mm ahead the load coil, the initial radiation zone exists and so any signal is not observed. In Fig 2 (a), lower emission intensity is observed for Mg(I) in presence of N_2 up to 15 mm from the load coil, considered the analytical zone of the ICP. However, the same behaviour is not observed for Mg(II), whose signal increases in presence of N_2. The same trend of signal increase and decrease as a function of the distance of the induction coil is observed for Mg(II) with and without N_2 addition. Similar behaviour of that of Mg(II) is observed for Ar(I) as can be seen in Fig. 2 (c). According to the results found, the foreign gas (N_2) seems to exert more relevant influence on the analytical zone of the ICP. The N_2 influence can be partially explained by the thermal conductivity of N_2, which is estimated to be 30 times higher than that of Ar at 8000 K.[1] Molecular nitrogen is probably predominant at lower distance from the load coil, which enhances the thermal conductivity and, therefore, improves, particles vaporization, atomization and ionization in the ICP locally. Atomic N^+ may be predominant at higher distances from the load coil and this species has similar thermal conductivity of Ar^+ - this prediction was confirmed by plasma robustness. Changes of the size and shape of the central channel of the ICP, caused by N_2, can also be responsible for the enhanced plasma-particle interaction, which justifies the utility of the mixed-gas-plasma source in the analysis of complex matrices. In Fig. 2 it is possible to observe that in both plasmas the emission signal is highest at 11 mm from the load coil. For higher N_2 flow, plasma constriction takes place (plasma shrinks), which can reduce the time for an effective interaction among plasma and sample particles. However, despite of that, it has been reported [1] that the interaction is enhanced in the mixed-gas plasma.

A simple way to monitor the effectiveness of atomization and ionization processes in the ICP is to measure the ratio Mg(II)-280.270 nm/Mg(I)-285.213 nm (plasma robustness) as detailed by Mermet.[44] The ionic to atomic ratio indicates how efficient is the energy transfer among the annulus of the hot plasma and the cold gas flow in the central channel. The ratio also provides insights of local thermodynamic equilibrium (LTE), whereas Mg(II)-280.270 nm/Mg(I)-285.213 nm ≥ 10 suggest low probability of plasma equilibrium shift when the sample matrix is introduced in the ICP (*i.e.* low probability of plasma-related matrix effects). Plasma robustness was measured for both Ar-ICP and N_2-Ar-ICP and the collected signals are illustrated in Fig. 3. With respect to the axial profile (Fig. 3 (a), it is observed that a non-robust plasma (Mg(II)/Mg(I) ≤ 6) was obtained for the Ar-ICP, caused by water removal in the desolvation step, which affects the thermal conductivity on the ICP. The situation was improved with the addition of N_2, as observed by the higher Mg(II)/Mg(I) ratio achieved. A more pronounced decrease of energy transfer is identified for the pure Ar-plasma when compared to the mixed-gas plasma, at 10 mm from the load. This can be directly related with the predominance of molecular nitrogen close the load coil. The N_2 molecule is dissociated in the central channel of the ICP at greater distances from the load coil, reducing the plasma robustness. Nonetheless, part of nitrogen remains as N_2 along the plasma axis and N_2 diffusion in the mixed gas plasma cannot be excluded. Thus, the N_2 effect would not be limited to the central channel of the ICP. The N_2 effect can be partially verified by the profile shown in Fig. 3 (b); for -5 to +5 mm from the central channel of the Ar-ICP the Mg(II)/Mg(I) ratio is lower than that observed for the mixed-gas plasma. This confirms the different coupling efficiency in presence of N_2. The ICP is about 2.5 times more robust by adding a low flow of N_2. Therefore, the added N_2 affects the induction zone that is the most energetic in the ICP, as observed by the increased plasma robustness close the load coil. It is worth citing that it

was not possible to obtain profiles broader than that shown in Fig 3 (b) because the aerosol flow was limited by the injector tube diameter.

Matrix effects

Challenges in ICP-spectrometry still include understanding of fundamental plasma parameters and elimination of matrix effects. These effects are observed when the concomitants of the sample matrix cause analyte signal suppression or enhancement, whose intensity will depend on analyte characteristics and sample matrix as well. In general, matrix effects can be categorized in two main types: sample introduction-related or plasma-related. While the former can, in some cases, be more easily corrected by means of alternative calibration strategies (standards addition, internal standardization, matrix-matching) or even matrix separation, the latter is usually unpredictable. In order to evaluate how the foreign gas (N_2) could reduce matrix effects, seawater (2 to 500 - fold diluted) was spiked with the analyte and its emission subsequently measured. More concentrated and more diluted seawater simulated complex and simple matrices, respectively. Fig. 4 illustrates the results obtained for diluted seawater. According to this figure, addition of N_2 does not exert any remarkable influence on the signal of the analyte for seawater diluted 50 - 500 times. The matrix effects observed may be related primarily to the sample introduction system (generation and transport of aerosol) in the ICP. Since these effects are more pronounced, they could hide those occurring in the ICP under the N_2 flow. As previously observed,[9] N_2 does not affect the sample-introduction (aerosol generation and transport) in the ICP, but solely the ICP atmosphere. In Fig. 4, signal suppression is observed for all analytes, excepting Sr (8,74 eV). As Sr is present at appreciable concentration in seawater (about 8000 mg L^{-1} in undiluted seawater), the signal suppression was probably compensated by the signal of Sr already present in the sample. Although seawater was very diluted, matrix effects were still observed. This occurred because a high efficiency nebulizer was used for introducing the sample solution in the ICP. That is, the amount of sample reaching the ICP is larger when compared to a conventional pneumatic nebulizer. The effect of N_2 became noticeable for seawater 2 to 10-fold diluted; it can be clearly seen that the analyte signal was less affected when N_2 was added to the ICP. Excluding Sr, the mean analyte signal suppression in the Ar-ICP was 56%, 63% and 71% for seawater 10 -, 5- and 2-fold diluted, respectively. On the other hand, in the Ar-N_2-ICP the mean analyte signal suppression was 42%, 48% and 52%, for seawater 10 -, 5- and 2-fold diluted, respectively. For the 2-fold diluted seawater, whose salinity is 17.5, the analyte signal suppression was 35% lower in the Ar-N_2-ICP. The reasons for the lower signal suppression would be the higher thermal conductivity of N_2, improving particles vaporization, especially for a such complex matrix. Nitrogen, by increasing the excitation temperature in the central channel of the ICP, would also mitigate shifts in the fundamental plasma parameters caused by the matrix components. The use of mixed-gas plasma combined with on-line flow injection were investigated in order to improve sample throughput in seawater analysis, as detailed by Beauchemin *et al.* [8, 11-16] The authors observed that the foreign gas (N_2) decreased the sensitivity (in comparison to the Ar-ICP). This drawback was possibly related with the excess of N_2 added, which could decrease the ICP temperature, time of plasma-particle interaction, and/or increase the population of doubly charged ions, decreasing the population of single charged ions and the sensitivity as a consequence. In addition, the nitrogen-species may have also increase the background signal.

Excitation temperature

Figure 5 shows the excitation temperatures estimated by measuring the signal of Fe(II) lines along the ICP axis. The temperature was calculated from the slope of the Boltzmann plot, whereas the correlation coefficients were higher than 0.99. The values quoted in Fig. 5 were calculated from measurements carried out at room temperature and significant discrepancies were possible inside the ICP environment at 8000 K. The deviations are related with Ar and N_2, whose properties are known at 25 ^oC in the room environment and extrapolated to 8000 K in the ICP environment. However, it can be stated that the calculated temperature is still reliable.[47] It is important to mention that all data were collected by using a sequential spectrometer, which may have deteriorated the precision (when compared to a simultaneous spectrometer) as denoted by the deviations in Fig. 5. As shown in this figure, the excitation temperature increased from 7480 K to 7910 K with the addition of N_2, which confirms that this molecular gas improves plasma characteristics (particularly in the central channel), not only by its higher thermal conductivity (0.024 W/mK for N_2 and 0.016 W/mK for Ar) but also by its higher heat capacity (1.04 kJ/kgK for N_2 and 0.52 kJ/kgK for Ar). In fact, it has been estimated that the thermal conductivity of N_2 is 30 times higher than that of Ar,[1] which explains the remarkable N_2 effect in tne Ar-ICP, even when a very low flow of N_2 is added. The plasma may depart from the LTE when N_2 is added, especially in the central channel. However, the present investigation was conducted using robust plasma conditions, ensuring that both plasmas moved closer the LTE. Therefore, this source of uncertainty was reduced. Other researchers[40] found that adding 10% of N_2 into the outer gas flow increased the temperature of the ICP to about 1000 K. Witte and Houk[49] observed that the gas kinetic temperature of the ICP increased 340 K when laser ablation was used as sample introduction system and 5 mL min^{-1} of N_2 was added to the carrier gas. Therefore, the results found in the present study corroborate with others already reported.

Figures of merit and accuracy

Addition of N_2 to the Ar-ICP gives rise to structural background owing to emission of molecular species such as N_2, N_2^+, NH and NO. Bands related with emission of NO at 200 to 280 nm are observed. The interval between 350 and 500 nm should be used because it is relatively free of interferences caused by nitrogen.[1,37] However, the wavelength of prominent lines of the investigated elements were lower than 280 nm. The intensity of spectral interference caused by N_2 were estimated by measuring the blank signal in both atmospheres, *i.e.*, with and without N_2 addition. In both cases, the signal of the analyte in calibration solutions was blank corrected and the slope of the

calibration curves compared to check the sensitivity. The results obtained are given in Table 3 where a pattern can be observed for atomic and ionic lines; the ratio "slope of calibration curve obtained with N_2 addition/slope of calibration curve obtained without N_2 addition" is typically < 1 for atomic lines. Therefore, the sensitivity for ionic lines increases by adding N_2 to the Ar-ICP. Remarkable exceptions are Sr(II) 407.771 and Ni(II) 232.003 that may behave as atomic lines. These results corroborate with the excitation temperature calculated using the Boltzmann equation and a set of Fe(II) emission lines. This means that ionization of analyte atoms increases with the temperature increase promoted by the low flow of N_2 introduced in the central channel of the ICP. It is interesting to observe in Table 3 that higher enhancement was observed for Zn(II) and Cd(II) whose ionization energies are 9.39 eV and 8.99 eV, respectively. These two species may participate in charge-transfer reaction with NO^+, whose ionization potential is 9.26 eV. The higher excitation temperature of the mixed-gas plasma leads to an overpopulation of ionic states, but charge transfer reaction with NO^+ may happen concomitantly in the ICP and would be the reason for the higher enhancement observed for Cd(II) and Zn(II). The linearity of calibration curves was not affected by N_2, as observed by the r^2 values in Table 3. The LODs were almost similar for the Ar-ICP and N_2-Ar-ICP. The LODs were calculated following the 3s criterion, whereas s is the standard deviation of ten consecutive blank measurements. According to the results obtained it can be stated that adding a low flow of N_2 to the Ar-ICP is a straightforward way to increase the ICP robustness without a visible side effect on the ICP performance.

Accuracy was accessed by analysing certified water (trace elements in natural water - NIST 1640a). The analyte concentration found agreed with that certified, indicating that the spectral interferences caused by adding N_2 to the Ar-ICP were properly blank corrected. Three certified sediment samples were analyzed to check accuracy for more complex matrices. As can be seen in Table 4, the concentrations found and those certified or informed were in agreement, which again confirms that there is not side effects by adding a small flow of N_2 in the central channel of the Ar-ICP. One can note in Table 4 that the concentrations measured were in general more accurate when the Ar-N_2-ICP was employed.

Investigation using diagnostic emission species

Changes of fundamental plasma parameters (*i.e.*, electron number density, excitation or ionization temperature, atom/ion population distribution) taking place in the central channel of the Ar-ICP under a low flow of N_2 are revealed by changes in the emission intensities of atomic and ionic lines. These effects are illustrated in Fig. 6 where one can see that the intensity of Mg(I) decreases while that of Mg(II) increases. According to Burton and Blades,[45] atomic Mg with low excitation energy may be excited by electron impact predominantly. The same does not occur for high-energy levels, which may be excited by charge-transfer reactions involving Ar^+ species, causing an overpopulation of ionic Mg. Although the emission intensity may be affected by changes in plasma temperature, the remarkable suppression of Mg(I) emission intensity that took place when N_2 was added to the Ar-ICP (see Fig. 6) denotes a decrease in the excitation pathway by electron impact. Sesi *et al.*[46] have demonstrated that a significant drop of electron number density occurs when N_2 is added to the central channel of the ICP. They attributed this phenomenon to the high heat capacity of N_2, which acts as a 'energy sink', storing energy from the plasma and further reducing electron density.

The enhancement of Mg(II) intensity shown in Fig. 6 suggests a possible overpopulation of Ar^+ (by charge-transfer from N_2^+ to Ar species), which would ionize Mg atoms. An evidence of such ionization mechanism that takes place in a Ar-N_2-ICP was experimentally demonstrated by Holliday and Beauchemin.[8] They added N_2 to the outer gas flow and through measurements of plasma background species in both ICP atmospheres and respective radial spatial profiles, demonstrated that charge-transfer reaction may be the predominant ionization path in the Ar-N_2-ICP, which is consistently different from electron impact in a pure Ar-ICP.

Additional investigations were conducted by monitoring emission signals of O(I) as well as OH radicals. These species are directly related with the amount of water introduced in the ICP and can provide additional insights on the effects of N_2. Fig. 7 shows the effect of N_2 on the emission intensity of O(I) and OH. The increase of O(I) emission denotes that the decomposition of water increases in the central channel of the ICP under the N_2 flow. On the other hand, the intensity of the OH radical does not change, which simply indicates that the amount of water introduced into the ICP remains constant. It is important to remark that the addition of a low flow N_2 to the nebulizer gas does not affect the aerosol generation and subsequent transport to the ICP, as previously observed.[9]

Excited Ar states play a important role in Penning ionization and, therefore, Ar emission is an useful indicator of N_2 effects going on in the Ar-ICP. Two groups of argon emission lines involving low-energy (13.25 to 13.50 eV) and high-energy (14.80 to 15.40 eV) levels are useful for that purpose.[48] However, it is difficult to measure the emission of Ar because the detector becomes saturated. This shortcoming can be circumvented by reducing the time of signal measurements. The ICP OES spectrometer used in the present study limits the minimum measurement time to 0.1 s. At this condition it was possible to measure the emission intensity of several Ar lines. This was set as a compromise condition because the precision worsens with the decreasing of the signal integration time. According to Fig. 8. a clear pattern is not observed but those Ar lines with higher excitation energy were less enhanced or even suppressed when N_2 was added. If defect energy of 0.5 eV is considered, the excitation of Ar with energy of 14.03 eV to 15.03 eV has high probability to occur directly *via* charge-transfer among N^+ (14.53 eV). As shown in Fig. 8, the signals of Ar lines whose energy is 14.03 eV to 15.06 eV increase more than the others in presence of the N_2 flow. On the other hand, argon with higher excitation energy (15.13 to 15.35

eV) would be excited by charge transfer among N_2^+ (15.58 eV). However, this excitation path probability involves two steps whose occurrence is lower. This phenomenon could be the reason for the lower enhancements of the energetic states of Ar with 15.13 to 15.35 eV (lines 543.999, 602.515, 603.213 and 604.323 nm). However, more experiments involving a larger number of Ar excited states as well as spatial profiles collected along and across the ICP axis are required to validate and support these conclusions. A rather complex excitation path is possible in the used mixed-gas plasma, which may involve several processes occurring spatially and temporally. Ions distribution determined using ICP-MS can be used as a complementary tool to probe possible excitation mechanisms, as already demonstrated by Beauchemin *et al.* [7,8,11-16,51]

Conclusions

A low flow of N_2 in the central channel of the Ar-ICP significantly increased the coupling efficiency among the bulk plasma and the central channel without sensitivity degradation in ICP OES. The excitation temperature in the central channel of the ICP increased, improving its performance. The analyte signal suppression caused by the seawater matrix was reduced when N_2 was added to the ICP, being a high efficiency nebulizer (pneumatic nebulization with aerosol desolvation) used as sample introduction system. Reduction of matrix interference is also expected for other complex matrices by adding a low flow of N_2 to the ICP and using the same sample introduction system, which improves the sensitivity. Nitrogen added in the central channel of the ICP plays an important role in energy transfer locally (at the central channel), but does not affect the outer regions of the ICP, indicating an improbable N_2 diffusion. This molecular gas can also act positively as a load buffer, increasing plasma robustness and minimizing matrix effects without sacrificing sensitivity. These benefits would be useful for sample introduction systems such as electrothermal vaporization (ETV), laser ablation (LA), and nanonebulizers. Water exerts a positive buffering in the Ar-ICP and when these sample introduction systems are used the minimum amount of water is introduced into the ICP. Thus, a low flow of N_2 could compensate the lack of water. By collecting axial and radial emission profiles along and across the plasma axis, it was possible to identify possible shifts of excitations conditions caused by N_2. Although additional studies are necessary to confirm specific excitation pathways, the present study found evidence of charge-transfer reactions among ground-state Ar species and ionized nitrogen species (N_2^+ and N^+). The results found confirm that the excitation/ionization mechanism in the N_2-Ar-ICP is shifted in comparison to the Ar-ICP. Future studies will also focus addition of a low flow of N_2 to the auxiliary and outer gas flows in an attempt to gain robustness without sacrificing detectability for both ICP OES and ICP-MS techniques.

Acknowledgements

The authors would like to thank CNPQ and CAPES for scholarships and FAPERGS for financial support.

Notes

Institute of Chemistry, Federal University of Rio Grande do Sul, Av. Bento Gonçalves, 9500, 91501-970 Porto Alegre, RS, Brazil.
E-mail: dircepoz@iq.ufrgs.br; Fax: +55 51 3308 7304; Phone: +55 51 3308 7215

***To whom correspondence should be addressed (Dr. D. Pozebon)**: dircepoz@iq.ufrgs.br

References

1. A. Montaser and R. L. Van Hoven, *CRC Crit. Rev. Anal. Chem.*, 1987, **18**, 45.
2. G. L. Scheffler and D. Pozebon, *Anal. Methods*, 2014, **6**, 6170.
3. R. S. Houk, A. Montaser and V. A. Fassel, *Appl. Spectrosc*., 1983, **37**, 425.
4. S. F. Durrant, *Fresenius J. Anal. Chem.,*1993, **347**, 389.
5. B. S. Sheppard and J. A. Caruso, *J. Anal. At. Spectrom*., 1994, **9**, 145.
6. A. Montaser, V. A. Fassel and J. Zalewski, *Appl. Spectrosc.,* 1981, **35**, 292.
7. C. Agatemor and D. Beauchemin, *Spectrochim. Acta, Part B*, 2011, **66**, 1.
8. A. E. Holliday and D. Beauchemin, *J. Anal. At. Spectrom.,* 2003, **18**, 289.
9. G. L. Scheffler and D. Pozebon, *Anal. Chim. Acta*, 2013, **789**, 33.
10. G. L. Scheffler, V. L. Dressler and D. Pozebon, *Food Anal. Methods*, 2013, **7**, 1415.
11. D. Beauchemin and J. M. Craig, *Spectrochim. Acta, Part B*, 1991, **46**, 603.
12. A. E. Holliday and D. Beauchemin, *J. Anal. At. Spectrom.,* 2003, **18**, 1109.
13. A. E. Holliday and D. Beauchemin, *Can. J. Anal. Sci. Spectrosc*. 2002, **47**, 91.
14. G. Xiao and D. Beauchemin, *Can. J. Anal. Sci. Spectrosc.*, 2001, **46**, 28.
15. J. M. Craig and D. Beauchemin, *J. Anal. At. Spectrom.*, 1992, **7**, 937.
16. A. E. Holliday and D. Beauchemin, *Spectrochim. Acta, Part B*, 2004, **59**, 291.
17. J. W. Lam and J. W. McLaren*, J. Anal. At. Spectrom*., 1990, **5**, 419.
18. E. H. Choot and G. Horlick, *Spectrochim. Acta, Part B,* 1986, **41**, 925.
19. J. W. H. Lam and G. Horlick, *Spectrochim. Acta, Part B,* 1990, **45**, 1313.
20. J. Wang, E. Hywel Evans and J.A. Caruso, *J. Anal. At. Spectrom.,* 1992, **7**, 929.
21. S. Branch, L. Ebdon, M. Ford, M. Foulkes and P. O'Neil, *J. Anal. At. Spectrom*., 1991, **6**, 151.
22. K. Akatsuka, J. W. McLaren, J. W. Lam and S. S. Berman, *J. Anal. At. Spectrom.,* 1992, **7**, 889.
23. C. Haraldsson, B. Lyven, P. Ohman and J. Munthe, *J. Anal. At. Spectrom.*, 1994, **9**, 1229.
24. C. J. Amarasiriwardena, N. Lupoli, V. Potula, S. Korrick and H. Hu, *Analyst*, 1998, **123**, 441.

25. K. Akatsuka, T. Suzuki, N. Nobuyama, S. Hoshi, K. Haraguchi, K. Nakagawa, T. Ogata and T. Kato, *J. Anal. At. Spectrom.*, 1998, **13**, 271.
26. E. Hywel Evans and L. Ebdon, *J. Anal. At. Spectrom*., 1990, **5**, 425.
27. M. Ford, L. Ebdon and S. J. Hill, *Anal. Proc*., 1992, **29**, 104.
28. K. Newman, P. A. Freedman, J. Williams, N. S. Belshaw and A. N. Halliday, *J. Anal. At. Spectrom*., 2009, **24**, 742.
29. M. J. Bloxham, P. J. Worsfold and S. J. Hill, *Anal. Proc.,* 1994, **31**, 95.
30. T. van der Velde-Koerts and J. L. M. de Boer, *J. Anal. At. Spectrom.,* 1994, **9**, 1093.
31. Y. Zhu, K. Inagaki, H. Haraguchi and K. Chiba, *J. Anal. At. Spectrom.* 2010, **25**, 364.
32. F. Laborda, H. J. Baxter, H. M. Crews and J. Dennis, *J. Anal. At. Spectrom*., 1994, **9**, 727.
33. E. Hywel Evans and L. Ebdon, *J. Anal. At. Spectrom*., 1989, **4**, 299.
34. S. J. Hill, M. J. Ford and L. Ebdon, *J. Anal. At. Spectrom*., 1992, **7**, 719.
35. S. F. Durrant, *Fresenius J. Anal. Chem*., 1994, **349**, 768.
36. M. Ohata, Y. Takaku, K. Inagaki, A. Hioki and K. Chiba, *Anal. Sci.* 2009, **25**, 161.
37. A. Montaser and J. Mortazavi, *Anal. Chem.,* 1980, **52**, 255.
38. M. Cai, D. A. Haydar, A. Montaser and J. Mostaghimi, *Spectrochim. Acta Part B*, 1997, **52**, 369.
39. S. E. O'Brien, J. R. Chirinos, K. Jorabchi, K. Kahen, M. E. Cree and A. Montaser, *J. Anal. At. Spectrom*., 2003, **18**, 910.
40. I. Ishii, D. W. Golightly and A. Montaser, *J. Anal. At. Spectrom.*, 1988, **3**, 965.
41. E. H. Choot and G. Horlick, *Spectrochim. Acta, Part B*, 1986, **41**, 935.
42. E. H. Choot and G. Horlick, *Spectrochim. Acta, Part B*, 1986, **41**, 907.
43. E. H. Choot and G. Horlick, *Spectrochim. Acta, Part B*, 1986, **41**, 889.
44. J. M. Mermet, *Anal. Chim. Acta,* 1990, **250**, 85.
45 L. L. Burton and M. W. Blades, *Spectrochim. Acta, Part B*, 1991, **46B**, 819.
46 N. N. Sesi, A. MacKenzie, K. E. Shanks, P. Yang and G. M. Hieftje, *Spectrochim. Acta, Part B*, 1994, **49**, 1259.
47. G. Kreuning and F. J. M. J. Maessen, *Spectrochim. Acta, Part B*, 1989, **44B**, 167.
48. G. C-Y. Chan and G. M. Hieftje, *Spectrochim. Acta, Part B*, 2007, **62**, 196.
49. T. M. Witte and R. S. Houk, *Spectrochim. Acta, Part B*, 2012, **69**, 9.
50. Z. Hu, S. Gao, Y. Liu, S. Hu, H. Chen and H. Yuan, *J. Anal. At. Spectrom*., 2008, **23**, 1093.
51.Y. Makonnen and D. Beauchemin, Spectrochim. Acta, Part B, 2014, **99**, 87.

JAAS

RSCPublishing

ARTICLE

Table 1 Instrumental and operating conditions of the ICP OES equipment and spectral lines monitored

Parameter	Setting		
RF applied power (W)	1500		
Argon flow rate (L min^{-1})	Outer: 15; intermediate; 0.2, nebulizer: 0.6		
Injector tube	Alumina (2 mm i.d.)		
Integration time (s)	5		
Sample uptake rate (mL min^{-1})	0.65		
N_2 flow rate (mL min^{-1})	20		
Plasma view	Axial or radial[a]		
Emission line (nm)	Potencial, eV		Energy Sum, eV
	Excitation (E)	Ionization (I)	E + I
Ba (II) 233.527	6.00	5.21	11.21
Cd (I) 228.802	5.41	8.99	14.40
Cd (II) 214.440	5.78	8.99	14.77
Co (II) 228.616	5.84	7.86	13.70
Cr (II) 267.716	6.18	6.77	12.95
Cr (I) 357.869	3.46	6.77	10.23
Zn (I) 206.200	6.01	9.39	15.40
Zn (II) 213.857	5.80	9.39	15.19
Pb (II) 220.353	7.37	7.42	14.79
Pb (I) 217.000	5.71	7.42	13.13
Sr (II) 407.771	3.04	5.70	8.74
Cu (I) 327.393	3.78	7.73	11.51
Cu (II) 224.700	8.23	7.73	15.96
Mn (II) 257.610	4.81	7.44	12.25
Ni (II) 231.604	6.39	7.64	14.03
Ni (II) 232.003	5.34	7.64	12.98
Mo (II) 202.031	6.13	7.10	13.23

I: atomic state; II: ionic state; a: radial view was used to obtain emission profiles only

Table 2 Iron wavelengths, respective excitation potentials, transition probabilities (A) multiplied by thre statistical weight of emission levels (g). The data were extracted from reference 47

Wavelength (nm)	Excitation Potencial (eV)	gA (x 10^8 s^{-1})
275.574	5.48	21.1
275.329	7.77	24.8
274.648	5.59	11.7
274.320	5.62	7.20
273.955	5.51	15.4
273.074	5.62	1.00
272.754	5.59	3.41
271.441	5.55	3.86
266.664	8.07	24.1
266.466	8.04	26.5
262.829	4.84	3.43
262.567	4.77	3.35
262.167	4.85	0.97
261.762	4.82	2.62
261.382	4.85	3.98
261.187	4.79	8.71
260.709	4.84	6.63
259.940	4.77	22.1
259.837	4.82	7.85
259.154	5.82	4.07
258.588	4.79	6.44
256.691	5.91	2.60
256.347	5.88	5.21
256.253	5.82	12.8

JAAS RSCPublishing

ARTICLE

Table 3 Limit of detection (LOD), slope of calibration curves and respective linear regression coefficient (r). The ratio of slopes is identified as Ar-N_2 -ICP/Ar-ICP. The LOD was calculated following the 3σ criterion (n = 10). All data were obtained using external calibration and axially-viewed plasma

Spectral line	LOD, μgL^{-1} (Ar-ICP)	LOD, μgL^{-1} (Ar-N_2 ICP)	Slope (Ar-ICP)	Slope (Ar-N_2 ICP)	Ratio of slopes	r^2 (Ar-ICP)	r^2 (Ar-N_2 ICP)
Mo II 202.031	1	1	62	78	1.2	0.9997	0.9994
Ba II 233.527	0.1	0.2	1062	1259	1.2	0.9999	0.9998
Cd I 228.802	0.1	0.2	913	677	0.74	0.9998	0.9998
Cd II 214.440	0.5	0.4	174	315	1.8	0.9998	0.9998
Co II 228.616	0.2	0.2	371	459	1.2	0.9999	0.9998
Cr II 267.716	0.2	0.3	450	572	1.3	0.9999	0.9998
Cr I 357.869	0.2	0.4	1663	825	0.49	0.9999	0.9999
V II 292.464	0.4	0.9	292	324	1.1	0.9999	0.9999
V II 290.880	0.3	0.2	856	935	1.1	0.9999	0.9999
Zn II 206.200	1	1	74	117	1.6	0.9934	0.9977
Zn I 213.857	0.5	0.4	485	426	0.87	0.9940	0.9922
Pb II 220.353	3	3	28	28	1.0	0.9997	0.9997
Pb I 217.000	16	28	5.1	3.6	0.71	0.9993	0.9977
Sr II 407.771	0.01	0.01	78610	68700	0.87	0.9999	0.9999
Cu I 327.393	0.1	0.2	1798	1664	0.92	0.9990	0.9987
Cu II 224.700	0.5	2	190	128	0.67	0.9990	0.9988
Mn II 257.610	0.02	0.02	6064	6930	1.1	0.9999	0.9999
Ni II 231.604	0.5	0.5	182	228	1.2	0.9997	0.9996
Ni II 232.003	0.9	1.0	84	68	0.81	0.9997	0.9996
Fe II 238.204	0.25	0.20	867	1042	1.2	0.9999	0.9998

JAAS

RSCPublishing

ARTICLE

Table 4 Analysis of certified reference samples. Concentrations values measured are the mean and standard deviation of three independent determinations (n = 3). External calibration and axially viewed plasma were used. Concentration in μg g^{-1}

Spectral Line	Soil			Pond Sediment			River Sediment		
	Certified	Measured Ar-N_2-ICP	Measured Ar-ICP	Certified	Measured Ar-N_2-ICP	Measured Ar-ICP	Certified	Measured Ar-N_2-ICP	Measured Ar-ICP
Mo 202.031	-	nd	nd	-	nd	nd	(0.64)	nd	nd
Ba 233.527	792 ± 36	773 ± 28	940 ± 50	-	245 ± 20	310 ± 30	(531)	530 ± 25	468 ± 20
Cd 228.802	12.3 ± 0.3	25 ± 1	51 ± 5	0.82 ± 0.06	nd	nd	0.533 ± 0.026	nd	nd
Cd 214.440	12.3 ± 0.3	11 ± 1	16 ± 3	0.82 ± 0.06	nd	nd	0.533 ± 0.026	nd	nd
Co 228.616	5.99 ± 0.14	4.5 ± 0.5	8.6 ± 1.0	27 ± 3	23 ± 2	30.3 ± 1.5	(19.4)	16.5 ± 1.2	20.7 ± 3.5
Cr 267.716	23 ± 6	19 ± 2	37.6 ± 3.0	75 ± 5	70 ± 4	75.5 ± 3.0	138 ± 7	137 ± 10	139 ± 21
Cr 357.869	23 ± 6	17.5 ± 1	21.7 ± 1.4	75 ± 5	68 ± 8	48.6 ± 2.0	138 ± 7	139 ± 12	136 ± 2.0
V 292.464	82 ± 9	75 ± 5	72 ± 8	(250)	230 ± 30	210 ± 15	(104)	45.2 ± 1.8	40.3 ± 3.5
V 290.880	82 ± 9	72 ± 3	68.3 ± 5.3	(250)	215 ± 25	218 ± 13	(104)	48.5 ± 1.5	42.5 ± 2.0
Zn 206.200	4180 ± 150	3980 ± 375	4540 ± 350	343 ± 17	325 ± 15	324 ± 11	142 ± 3	138 ± 10	118 ± 16
Zn 213.857	4180 ± 150	4175 ± 380	4580 ± 240	343 ± 17	320 ± 10	325 ± 9	142 ± 3	135 ± 12	114 ± 10
Pb 220.353	5550 ± 30	5640 ± 330	5320 ± 150	105 ± 6	103 ± 4	120 ± 4	42.3 ± 1.6	40.3 ± 2.1	28 ± 2
Pb 217.000	5550 ± 30	5660 ± 530	5240 ± 450	105 ± 6	181 ±13	334 ± 21	42.3 ± 1.6	45.2 ± 2.3	52 ± 4
Sr 407.771	255 ± 7	275 ± 15	310 ± 20	(110)a	120 ± 23	160 ± 25	(235.2)a	240 ± 13	253 ± 27
Cu 327.393	3420 ± 50	3462 ± 50	3360 ± 190	210 ± 12	220 ± 10	186 ± 20	44.1 ± 1.0	41.5 ± 1.4	42.5 ± 6.0-
Cu 224.700	3420 ± 50	3340 ± 85	3570 ± 250	210 ± 12	218 ± 14	208 ± 15	44.1 ± 1.0	42 ± 3	48.8 ± 3.4
Mn 257.610	2140 ± 60	1945 ± 125	2180 ± 40	(770)a	710 ± 25	760 ± 35	(737)a	732 ± 10	603 ± 25
Ni 231.604	8 ± 1	6.5 ± 1.0	10.5 ± 2.0	40 ± 3	38 ± 4	23.3 ± 2.0	75.2 ± 1.4	70 ± 2	47 ± 4
Ni 232.003	8 ± 1	6.0 ± 0.8	9.5 ± 1.3	40 ± 3	42 ± 3	40 ± 2	75.2 ± 1.4	78.3 ± 2.2	74.3 ± 4.5
Fe 238.204 b	4.32 ± 0.08	4.26 ± 0.18	4.38 ± 0.06	6.53 ± 0.35	6.39 ± 0.08	6.64 ± 0.27	(4.48)a	4.37± 0.03	4.13 ± 0.04

nd: not detected (see Table 3); a: informed value; b: concentration in %.
Soil: NIST 2710a; river sediment: BCR-320; pond sediment: NIES-2.

JAAS RSCPublishing

ARTICLE

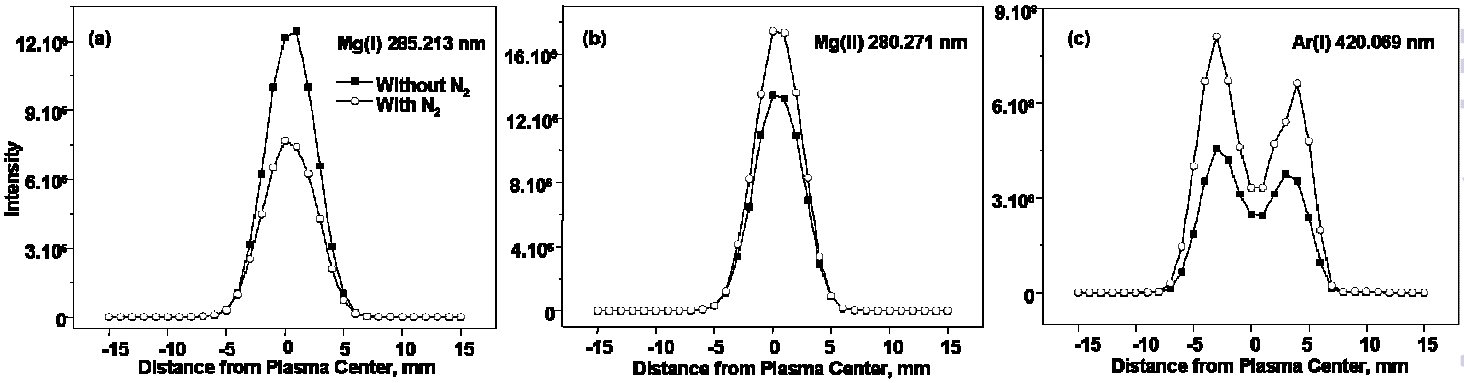

Fig. 1 Emission profiles for Mg(I), Mg(II) and Ar(I) collected across the ICP, with and without addition of N_2. Point 0 (x axis) identifies the central channel of the ICP, which was axially viewed.

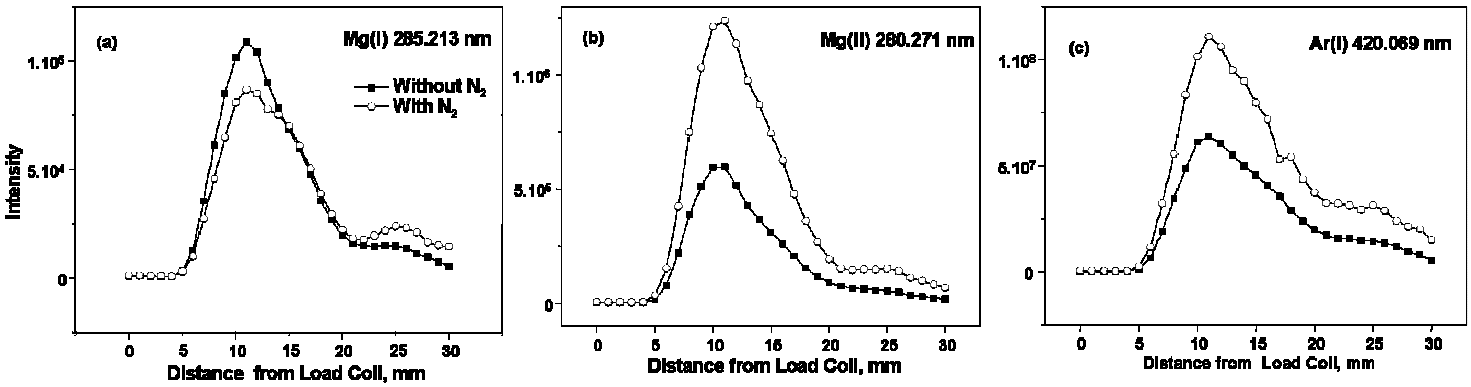

Fig. 2 Emission profiles for Mg(I), Mg(II) and Ar(I) collected along the ICP, with and without the addition of N_2. Point 0 (x axis) identifies the load coil position. The ICP was laterally viewed.

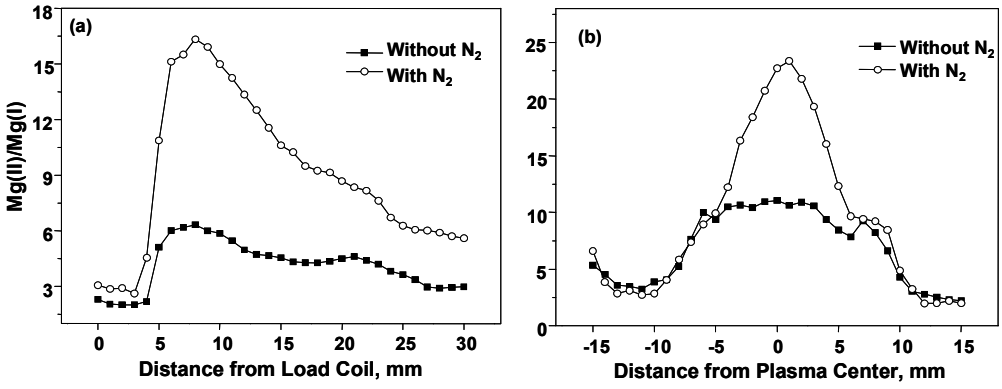

Fig. 3 Profiles of plasma robustness (Mg(II)/Mg(I)) along (a) and across (b) the ICP, with and without N_2 addition. The ICP was laterally viewed in (a) and axially viewed in (b). Point 0 (x axis) in (a) identifies the load coil position and in (b) it does the central channel of the ICP.

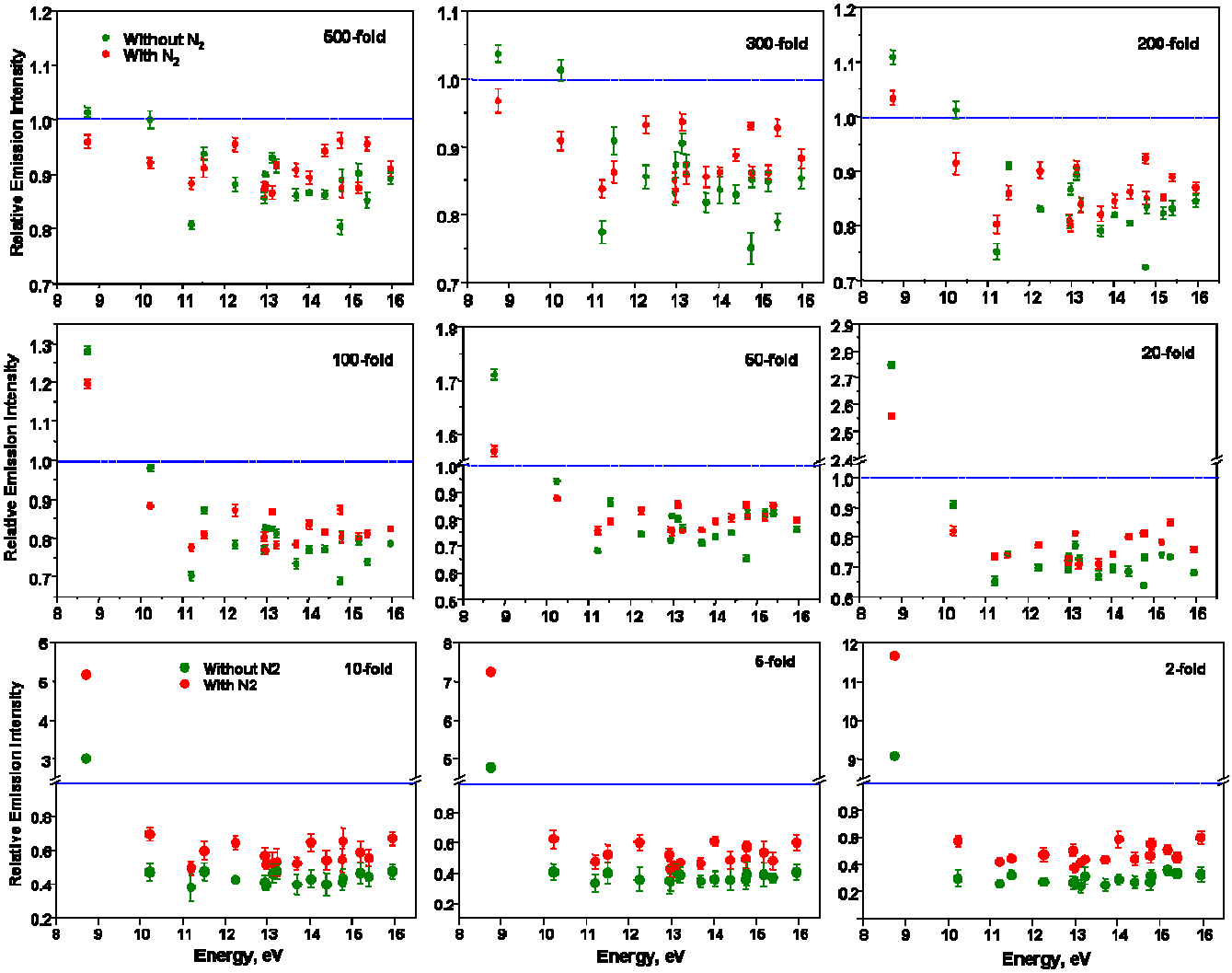

Fig. 4 Matrix effects of diluted sea-water spiked with 100 µg L^{-1} of elements cited in Table 1, with and without N_2 addition. The relative emission intensity in the y axis is the ratio analyte signal in HNO_3 5% (v/v)/analyte signal in diluted seawater. Ratio close to 1.0 identifies absence of matrix effect. The relative emission intensity is plotted against the energy sum (see Table 1). Error bars are the standard deviation of 3 independent measurements in axially-viewed ICP.

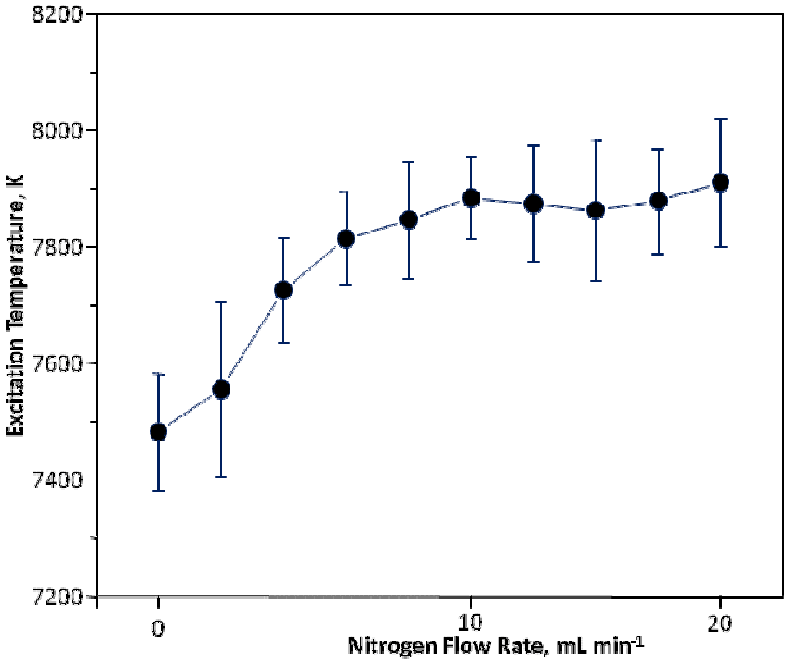

Fig. 5 Plasma excitation temperature calculated in the central channel of the ICP using Fe as thermometric species, as a function of the N_2 flow rate (added to the nebulizer gas). Error bars are the standard deviation of 3 determinations in axially-viewed ICP.

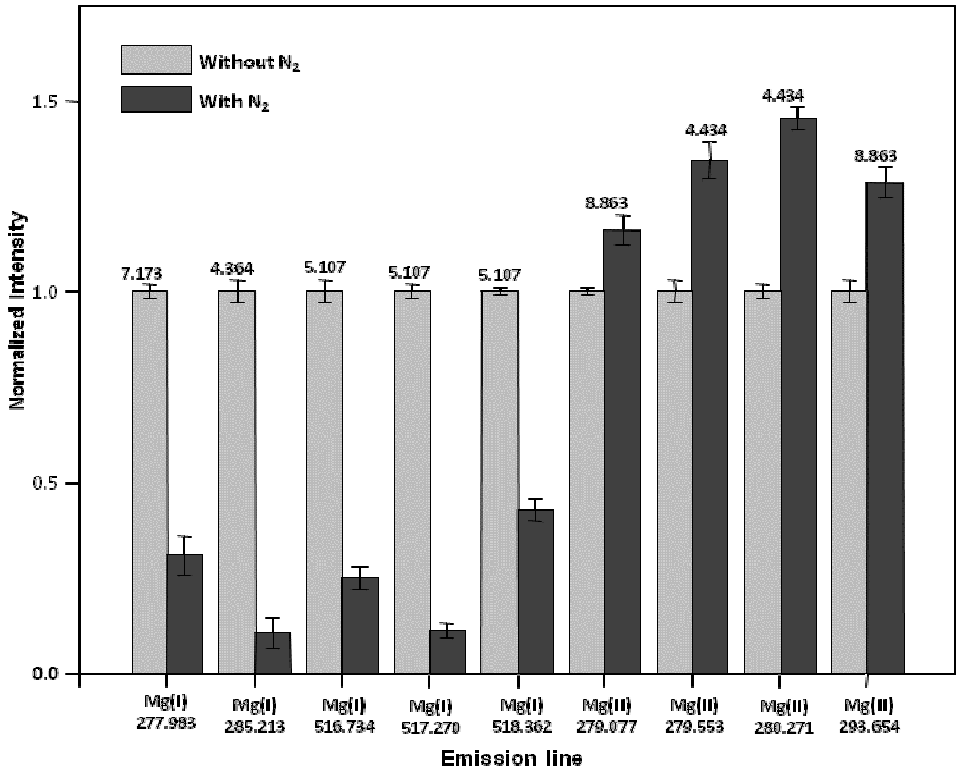

Fig. 6 Effect of N_2 (20 mL min^{-1} added to the nebulizer gas) on the intensity of atomic and ionic lines of Mg. The number above each bar is the respective excitation energy in eV.[45] Error bars are the standard deviation of 3 determinations in axially-viewed ICP.

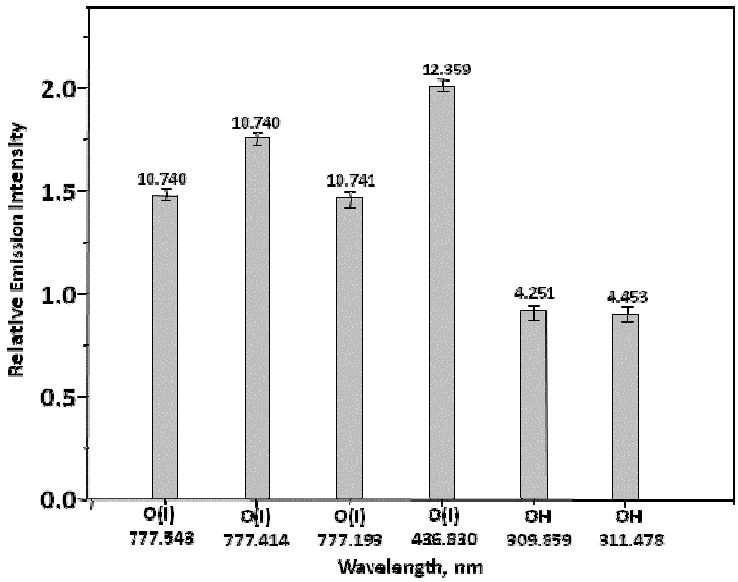

Fig. 7 Effect of N_2 (20 mL min^{-1} added to the nebulizer gas) on the emission intensity of atomic lines of oxygen and OH radical. The number above each bar is the respective excitation energy in eV. Values in the y axis are the ratio "signal in presence of N_2/signal in absence of N_2". Error bars are the standard deviation of 3 determinations in axially-viewed ICP.

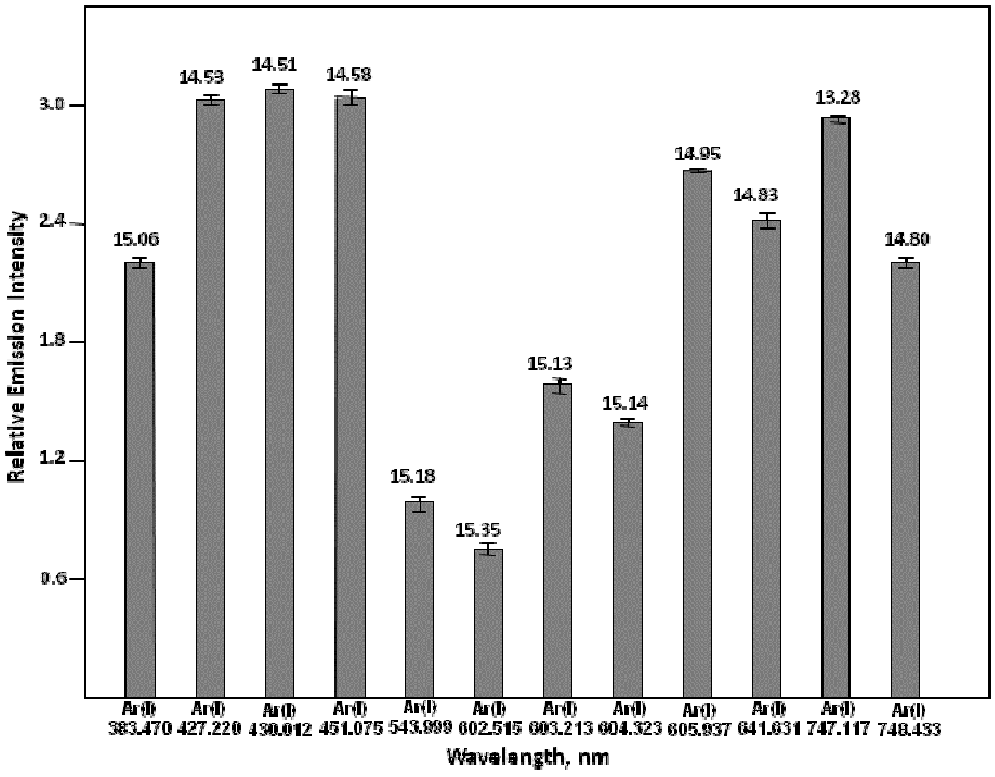

Fig. 8 Effect of N_2 (20 mL min^{-1} added to the nebulizer gas) on the signal enhancement of Ar-emission lines. The number above each bar is the respective excitation energy in eV. Values in the y axis are the ratio "signal in presence of N_2/signal in absence of N_2". Error bars are the standard deviation of 3 determinations in axially- viewed ICP.

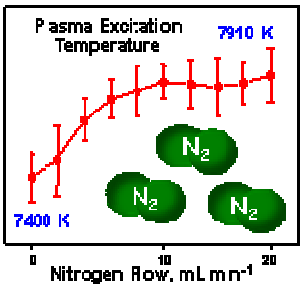

A low flow of N_2 introduced in the central channel of the Ar-ICP increases the excitation temperature and coupling efficiency among the bulk plasma and its central channel, improving the ICP robustness and respective performance.